CHEMISTRY OF MATERIALS

Article

pubs.acs.org/cm

Novel *Pn* Polymorph for Li_2MnSiO_4 and Its Electrochemical Activity As a Cathode Material in Li-Ion Batteries

Hugues Duncan, Abhinay Kondamreddy, Patrick H.J. Mercier, Yvon Le Page, Yaser Abu-Lebdeh,* Martin Couillard, Pamela S. Whitfield, and Isobel J. Davidson

National Research Council Canada, 1200 Montreal Rd, Ottawa, Ontario Canada K1A 0R6

ABSTRACT: We report on the synthesis and characterization of a new metastable polymorph of Li_2MnSiO_4 adopting the *Pn* space group, prepared by ion-exchange from Na_2MnSiO_4. Density-functional theory methods were used to predict the lattice parameters and atom positions of the new polymorph material and those of Na_2MnSiO_4 and $LiNaMnSiO_4$, allowing their identification by X-ray diffraction profiles, as well as the comparison of the measured and calculated cell parameters. The electrochemical activity of this new polymorph as a cathode material for lithium ion batteries was evaluated in coin cells and compared to that of the thermodynamically stable $Pmn2_1$ polymorph of Li_2MnSiO_4, as well as $LiNaMnSiO_4$ and Na_2MnSiO_4. Carbon coating, very vital to the electrochemical activity of the material, was added in situ to the material before ion-exchange because the metastable polymorph converts to the stable polymorph above 370 °C, as confirmed by differential scanning calorimetry scans. Both Li_2MnSiO_4 polymorphs display similar charge−discharge curves, except for a marginally lower lithium extraction voltage during the first charge of the *Pn* structure that may be due to the presence of sodium ion impurities. A discharge capacity of 110 mA h g^{-1} is initially observed for both Li_2MnSiO_4 polymorphs and both exhibit similar capacity fades. $LiNaMnSiO_4$, however, yields a stable capacity of 45 mA h g^{-1}, whereas Na_2MnSiO_4 yields an initial capacity of 20 mAh g^{-1}, increasing to 60 mAh g^{-1} with cycling.

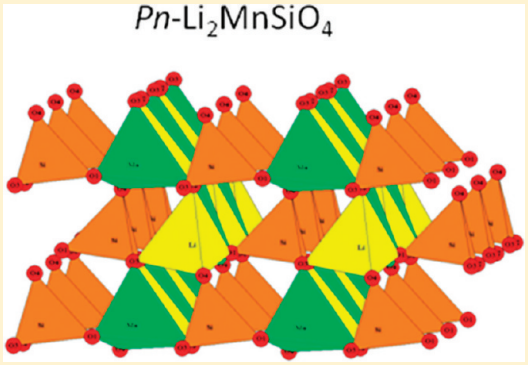

KEYWORDS: *lithium manganese silicate, polymorphism, Li-ion battery*

1. INTRODUCTION

Orthosilicates of transition metals with the general formula Li_2MSiO_4 (M = Fe, Mn, Co) have recently attracted attention as possible cathode materials for lithium-ion batteries.[1,2] The possibility of exchanging two lithium atoms per formula corresponds to theoretical capacities in excess of 300 mA h g^{-1}. This considerable enhancement in capacity combined with the greater stability of silicate materials, expected from the greater strength of the Si−O bond relative to the P−O bond of olivines ($LiMPO_4$), could hardly fail to create interest. The silicate family is known to be rich in polymorphs: Li_2FeSiO_4 has at least three reported polymorphs,[3−5] as have Li_2CoSiO_4[6] and Li_2MnSiO_4.[4,7,8] Two of the three known polymorphs of Li_2MnSiO_4 are orthorhombic (*Pmnb* and $Pmn2_1$), whereas the third is monoclinic ($P2_1/n$).[8] Ab initio density-functional theory (DFT) calculations have shown that both orthorhombic structures are more stable than the monoclinic one.[9]

As shown by Sirisopanaporn et al.[10] for Li_2FeSiO_4 and by Lyness et al.[11] for Li_2CoSiO_4, the crystal structure is known to have an influence on the electrochemical behavior. While Li_2FeSiO_4 shows good reversibility and stable capacity upon cycling, only one of the two lithium atoms per formula (M^n/M^{+n+1}) can be reversibly extracted and its operation voltage is relatively low at 2.8 V. Li_2CoSiO_4 has a higher operation voltage, but at 4.9 V, the extraction potential of the second lithium is above the oxidation potential of most known conventional electrolytes.[11] Most of the electrochemical data reported on Li_2MnSiO_4 is about the $Pmn2_1$ polymorph which is readily obtainable by sol−gel[12] and hydrothermal[7] synthesis techniques. The oxidation potential for the first and second lithium of $Pmn2_1$ Li_2MnSiO_4 are close and within the electrolyte electrochemical window (4.2 V and 4.4 V),[2] which allows for higher capacity. However, serious capacity loss upon cycling is a problem[4] because of instability of the delithiated material. In order to circumvent this capacity fading, we accordingly wish to explore here the possibility that other polymorphs of Li_2MnSiO_4 would be stable in the delithiated state.

Single-step synthetic routes like sol−gel, solid-state, and hydrothermal methods will only lead to the thermodynamically stable phases. However, methods are known for obtaining new metastable polymorphs by exchanging ions, starting from a similar material for which the stable structure is different. A well-known example is the synthesis of layered $LiMnO_2$ through Li-ion exchange on $NaMnO_2$ using solution[13] or molten salts[14] routes. In the case of metal silicates, Na_2MnSiO_4 is readily obtained in the *Pn* structure. As demonstrated in this paper, a simple ion exchange technique can then be used to

Received: September 16, 2011
Revised: November 10, 2011
Published: November 11, 2011

produce metastable Li_2MnSiO_4 or half exchanged $NaLiMnSiO_4$ without altering the *Pn* space group of Na_2MnSiO_4.

In this paper, we report the first synthesis and characterization of *Pn*-Li_2MnSiO_4 along the above lines by performing Li-ion exchange on *Pn*-Na_2MnSiO_4. Ab initio DFT calculations[15] are performed on the expected reaction products, allowing their identification by X-ray diffraction profiles, as well as the comparison of the measured and calculated cell parameters. DFT calculations were also used to predict the lithium extraction voltages and stability of the polymorphs. It will be shown that the delithiated form of the new polymorph is predicted to be more stable than its delithiated thermodynamic polymorph counterpart, presumably because of the framework structure of the *Pn* polymorph in the delithiated state vs the layered structure adopted by the $Pmn2_1$ polymorph. In addition, we report on the electrochemical activity of Na_2MnSiO_4, $LiNaMnSiO_4$ and Li_2MnSiO_4 in lithium cells and compare it to the thermodynamically stable $Pmn2_1$ polymorph.

2. METHODOLOGY

2.1. Synthesis. *2.1.1. Synthesis of Pn-Na_2MnSiO_4.* Na_2MnSiO_4 was synthesized by a sol−gel method. Sodium acetate and manganese acetate (Aldrich) were dissolved in deionized water and added to a solution of tetraethylorthosilicate (TEOS) (Aldrich) in ethanol. The pH was adjusted to 2 by addition of acetic acid and the solution was heated at 65 °C until full evaporation of the solvent. Carbon coated Na_2MnSiO_4 was obtained by adding sucrose to the solution before drying. The dry powder was crushed in a mortar and pressed before sintering at 700 °C for 12 h (2 °C/min heating and 5 °C/min cooling rate) under flowing argon with 5% H_2.

2.1.2. Ion-Exchanging Na_2MnSiO_4. Two methods of ion exchange were used. The first was performed by refluxing Na_2MnSiO_4 with a large excess of LiBr in hexanol for 4 h − 12 h.[13] In the second, Na_2MnSiO_4 powder was added to an aqueous solution of LiBr at 165 °C for 17 h in a hydrothermal reactor. In both cases, the solution was filtered and the powder was then washed with ethanol and dried overnight at 60 °C.

2.1.3. Synthesis of $Pmn2_1$-Li_2MnSiO_4. The $Pmn2_1$ polymorph of Li_2MnSiO_4 was obtained by the same sol−gel synthesis method as for Na_2MnSiO_4 using lithium acetate (Aldrich) instead of sodium acetate and following the same heat treatment. Carbon-coated $Pmn2_1$-Li_2MnSiO_4 was also obtained by adding sucrose to the solution before drying the solution at 65 °C.

2.2. Materials Characterization. *2.2.1. X-ray Diffraction.* X-ray diffraction powder patterns were collected by a Bruker D8 X-ray diffractometer with a Cu Kα tube in the range 15−90° and steps of 0.02° using a scintillation detector with graphite monochromator. The counting time was between 14 and 28 s depending on the sample. Variable divergence and antiscattering slits corresponding to 12 mm or 20 mm beam length were used, depending on the sample. Lattice parameters were obtained from Rietveld refinement[16] of XRD pattern using TOPAS 4.2.[17]

2.2.2. Differential Scanning Calorimetry (DSC). Differential scanning calorimetry was performed with TA Instruments DSC model 2920 using nitrogen as the flowing gas. For the measurements, 10 mg of sample was weighed in aluminum pans. The powders were dried in a vacuum oven overnight before the measurements. The temperature was equilibrated at 100 °C before scanning at 20 to 500 °C. The instrument was calibrated using indium and lead as standards immediately before the measurements.

2.2.3. SEM and TEM imaging and EDX analyses. SEM was carried on powders using a JEOL 840A microscope. TEM specimens were prepared by first dispersing the powder in ethanol, sonicating for a few minutes, and depositing a few drops of the solution on lacey-carbon grids. A 200 keV JEOL JEM-2100F TEM equipped with a CCD camera (Gatan UltraScan 1000) and an Oxford INCA EDX was used for this study.

2.2.4. Bulk Elemental Composition Analyses. Bulk elemental analyses of synthesis products were obtained by X-ray fluorescence (XRF) spectrometry. The lithium borate fusion method was used to prepare the specimens and calibration standards as fused beads. 100 mg of sample were mixed with 7 g of flux. The type of flux used was Claisse 66.67%$Li_2B_4O_7$−32.83%$LiBO_2$ −0.5%LiBr. The mixtures were fused with a Claisse M4 three-position gas fluxer producing 32-mm fused beads. An automated Bruker AXS S4 Pioneer was used to analyze all of the specimens. The S4 pioneer is a 4 kW sequential wavelength-dispersive XRF spectrometer using a Rh-anode X-ray tube with 75 m thin Be end window. All the measurements were done under vacuum mode using a 28 mm mask and a 0.23 degree collimator. Calibration curves were developed for analysis of battery-related materials and used to determine the elemental concentrations of 7 major elements (Mn, Ni, Ti, Co, Fe, Si and Zn) in the bulk synthesis products. The calibration curves built for each element were based on linear regressions of net intensity count rates measured from >10 calibration standards for each element. The calibration standards consisted of high-purity oxides (MnO, NiO, TiO_2, CoO, Fe_2O_3, SiO_2, and ZnO).

2.3. Ab initio DFT Calculations. *2.3.1. Optimization of Crystal-Structure Models.* DFT-optimized crystal structures of Na_2MnSiO_4, Li_2MnSiO_4, $LiMnSiO_4$ and $MnSiO_4$, as well as those of the two possible orderings of $LiNaMnSiO_4$ in space group *Pn* were derived from those of *Pn*-Ag_2ZnSiO_4.[18] DFT-optimized crystal structures were also obtained in the $Pmn2_1$ space group for all these chemical compositions. The crystal-structure optimizations were performed with VASP[19,20] using the exchange and correlations energies calculated under the generalized gradient approximation (GGA). All calculations used spin polarization according to the scheme of Vosko, Wilk and Nusair[21] and a 6 × 6 × 6 k-mesh. For selected cases, to more accurately evaluate total-energy differences between distinct polymorphs were also performed, GGA+U calculations including the Hubbard parameter correction. All other optimization parameters were as detailed in Mercier and Le Page.[22] Creation of all VASP input data files as well as all interpretation of VASP output files was performed with Materials Toolkit.[23]

2.3.2. Electrochemical Voltage Calculations. Ab initio GGA+U DFT energies were calculated with VASP for Li_2MnSiO_4, $LiMnSiO_4$, $NaMnSiO_4$, $LiNaMnSiO_4$ and delithiated $MnSiO_4$ in space groups *Pn* and $Pmn2_1$. Following Arroyo-de Dompablo et al.[9] in their calculations on the $Pmn2_1$ polymorph of Li_2MnSiO_4, we used a uniform value of 5 for the quantity $U-J$ of tetrahedral Mn for the three compounds. We then analyzed total energies for those materials with eq 1 in Zhou et al. (2004)[24] using a total energy of −1.891 eV that we calculated for Li_{metal} with a k-mesh of 23 × 23 × 23.

2.4. Electrochemical Testing of Battery Performance. For electrochemical testing, the material was first cast on an

dx.doi.org/10.1021/cm202793j | Chem. Mater. 2011, 23, 5446−5456

aluminum foil. This cast consisted of 80% active material, 5% Super S (Timcal Graphite and Carbon, Switzerland), 5% KS-4 graphite (KG, Lonza G+T, Switzerland) and 10% PVDF (Kynarflex 2800) binder dissolved in NMP (Anhydrous, 99%, Aldrich). The cast was dried in a convection oven at 85 °C and overnight in a vacuum oven at 80 °C. Li disks with 15.75 mm diameter were used as anode, and 12.7 mm diameter disks of cathode cast were punched. The electrochemical performance of the material was determined by cycling in 2325-type coin cells. Cells were assembled in an argon-filled glovebox. Celgard 2500 separators wetted with 1 M $LiPF_6$ (Sigma-Aldrich, 99.99%) in 3:7 EC:DEC (Sigma-Aldrich, 99%) was used as electrolyte. Coin cells were cycled using an Arbin cycler and cyclic voltammetry was carried out using a Bio Logic VMP3.

3. RESULTS

3.1. DFT Modeling for Na_2MnSiO_4, Li_2MnSiO_4 and $LiNaMnSiO_4$. The cell data and atomic positions results of DFT modeling for Na_2MnSiO_4, Li_2MnSiO_4 and $LiNaMnSiO_4$ are shown respectively in Tables 1, 2, and 3. Results from both GGA and GGA+U ab initio DFT calculations are shown. GGA and GGA+U values for lattice parameters *a*, *b*, and *c* agree with each other to about 0.01−0.05 Å while the monoclinic cell angle β values agree to within 0.06−0.18°. Fractional atomic coordinates agree together at the third decimal place between GGA and GGA+U values. This shows that spin-polarized GGA calculations produce sufficiently reliable crystal-structure predictions of lattice parameters and atom coordinates.

On the other hand, GGA+U ab initio DFT calculations including the Hubbard parameter correction U are required to correctly evaluate equilibrium voltages in a Li-ion battery.[2] Results for GGA+U calculated voltages are shown in Table 4. The similarity between voltage values derived ab initio and reported for the *Pn* and $Pmn2_1$ polymorphs is striking. The measured value of 4.2 V for the $Pmn2_1$ phase reported by Arroyo et al.[2] for extracting the first Li atom matched reasonably well with their calculated value of 4.12 V and our value of 4.23 V calculated in this work.

Finally, Table 5 compiles the total energies obtained by GGA +U ab initio calculations for Na_2MnSiO_4, Li_2MnSiO_4, $LiMnSiO_4$, and Li_2MnSiO_4 structures in both *Pn* and $Pmn2_1$ space groups. As expected, the structures with lower total energies are the thermodynamically stable phases which are observed experimentally to be formed by single-step sol−gel, solid-state, or hydrothermal synthesis methods; namely *Pn* for Na_2MnSiO_4 and $Pmn2_1$ for Li_2MnSiO_4. Further, calculated total energies indicate that $LiMn^{III}SiO_4$ is slightly more stable in the $Pmn2_1$ form. In contrast, $MnSiO_4$ is more stable in the *Pn* form, presumably due to the 3-D connectivity of MnO_4 and SiO_4

Table 1. Crystal-Structure Description of Na_2MnSiO_4, Space Group *Pn*

	a (Å)	*b* (Å)	*c* (Å)	β (deg)	
	6.9587	5.5859	5.2916	89.818	GGA
	6.9637	5.6101	5.2988	89.780	GGA+U
	7.0395(8)	5.5816(6)	5.3305(5)	89.82(3)	experimental
atom	Wyckoff position	*x*	*y*	*z*	
Mn	2a	0.00686	0.18164	0.00361	GGA
		0.00703	0.18197	0.00296	GGA+U
Si	2a	0.25315	0.68307	0.00871	GGA
		0.25329	0.68291	0.00867	GGA+U
Na	2a	0.75497	0.66966	−0.00627	GGA
		0.75503	0.66776	−0.00664	GGA+U
Na	2a	0.49965	0.18076	−0.00271	GGA
		0.49926	0.18336	−0.00227	GGA+U
O	2a	0.73263	0.60055	0.42587	GGA
		0.73533	0.59883	0.42314	GGA+U
O	2a	0.55872	0.16843	0.42251	GGA
		0.55875	0.17101	0.42030	GGA+U
O	2a	0.94892	0.20455	0.37843	GGA
		0.94979	0.20158	0.38433	GGA+U
O	2a	0.27410	0.70260	0.31786	GGA
		0.27051	0.70068	0.31751	GGA+U

Table 2. Crystal-Structure Description of Li_2MnSiO_4, space group *Pn*

	a (Å)	*b* (Å)	*c* (Å)	β (deg)	
	6.2162	5.3912	4.9742	89.898	GGA
	6.2580	5.4243	4.9749	89.834	GGA+U
	6.593(5)	5.402(1)	5.090(2)	89.7(3)	experimental
atom	Wyckoff position	*x*	*y*	*z*	
Mn	2a	0.00795	0.16426	0.00168	GGA
		0.00809	0.16473	−0.00095	GGA+U
Si	2a	0.25317	0.66883	0.00713	GGA
		0.25322	0.66825	0.00715	GGA+U
Li	2a	0.75354	0.65647	0.00128	GGA
		0.75373	0.65398	0.00104	GGA+U
Li	2a	0.50153	0.17880	0.00211	GGA
		0.50156	0.18302	0.00200	GGA+U
O	2a	0.75993	0.61785	0.39514	GGA
		0.76262	0.61606	0.39418	GGA+U
O	2a	0.53413	0.19436	0.39297	GGA
		0.53515	0.19764	0.39213	GGA+U
O	2a	0.97095	0.17864	0.41009	GGA
		0.96967	0.17659	0.41509	GGA+U
O	2a	0.24780	0.67158	0.33761	GGA
		0.24496	0.67015	0.33736	GGA+U

Table 3. Crystal-Structure Description of $LiNaMnSiO_4$, Space Group *Pn*

	a (Å)	*b* (Å)	*c* (Å)	β (deg)	
	6.8040	5.2931	5.0735	89.743	GGA
	6.7593	5.3850	5.0920	89.919	GGA+U
	6.854(1)	5.3932(7)	5.1332(7)	90.32(3)	experimental
atom	Wyckoff position	*x*	*y*	*z*	
Mn	2a	0.00683	0.17647	−0.00093	GGA
		0.00845	0.17069	−0.00076	GGA+U
Si	2a	0.25310	0.68689	0.01024	GGA
		0.25297	0.68631	0.00996	GGA+U
Na	2a	0.75319	0.67968	−0.00963	GGA
		0.75341	0.66878	−0.00940	GGA+U
Li	2a	0.50146	0.17855	0.00372	GGA
		0.50112	0.17952	0.00369	GGA+U
O	2a	0.75798	0.61879	0.44425	GGA
		0.75928	0.61393	0.44183	GGA+U
O	2a	0.55572	0.18487	0.38147	GGA
		0.55444	0.18837	0.37964	GGA+U
O	2a	0.95138	0.17384	0.39364	GGA
		0.95264	0.17248	0.39948	GGA+U
O	2a	0.24811	0.72708	0.33258	GGA
		0.24546	0.72432	0.33090	GGA+U

dx.doi.org/10.1021/cm202793j | *Chem. Mater.* 2011, 23, 5446−5456

Table 4. Calculated De-Lithiation Voltages for Li_2MnSiO_4 and $LiNaMnSiO_4$ with Respect to a Li Electrode (VASP GGA DFT+U)

polymorph	source	Li_2MnSiO_4 to $LiMnSiO_4$ (Mn^{2+} to Mn^{3+}) (V)	$LiMnSiO_4$ to $MnSiO_4$ (Mn^{3+} to Mn^{4+}) (V)
Pn	calcd here	4.25	4.50
Pn	meas here	3.9−4	
$Pmn2_1$	calcd here	4.23	4.53
$Pmn2_1$	meas here	4.2	
$Pmn2_1$	calcd †	4.2	4.48
$Pmn2_1$	meas ‡	4.12	
material	source	$LiNaMnSiO_4$ to $NaMnSiO_4$ (Mn^{2+} to Mn^{3+}) (V)	
Pn $LiNaMnSiO_4$	calcd here	4.02	
Pn $LiNaMnSiO_4$	meas here	4.2	

†Value read off Figure 2 in ref 2. ‡Value read off Figure 3 in ref 2.

Table 5. Total Energies Obtained by GGA+U Ab initio Calculations

	total energy (eV per formula unit)			
polymorph	Na_2MnSi0_4	Li_2MnSi0_4	LiMnSiO4	MnSiQ4
Pn	−105.338	−110.056	−97.778	−85.048
Pmn 2_1	−104.570	−110.098	−97.857	−84.855
difference (kJ/mol*):	−81.5	4.1	7.8	−19.0

*1 eV per formula unit =96.487 kJ/mol.

tetrahedra in the *Pn* structure compared to layered architecture in the $Pmn2_1$ form, as shown in Figure 1.

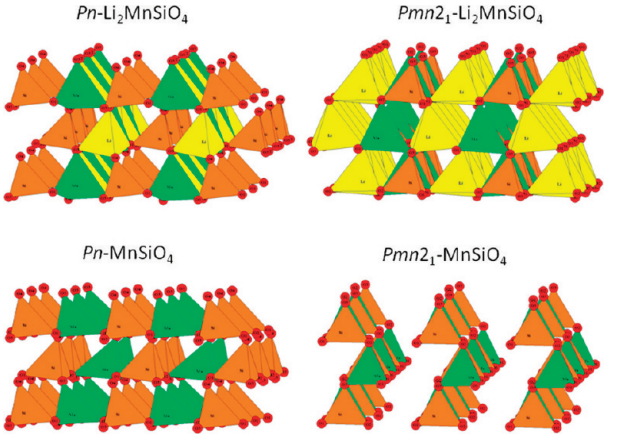

Figure 1. Polyhedral representations of the crystal structures of Li_2MnSiO_4 and $MnSiO_4$ in *Pn* and $Pmn2_1$ space groups. LiO_4, MnO_4 and SiO_4 tetrahedra are shown, respectively, in yellow, green, and orange.

3.2. XRD Characterization of Synthesis Products.

Figure 2 shows the experimental X-ray powder diffraction patterns for the reaction products of three successful syntheses of nearly single-phase material. Figure 2a corresponds to the Na_2MnSiO_4 product obtained using the sol−gel synthesis procedure described above followed by sintering at 700 °C for 12 h under flowing argon with 5% H_2. Figure 2b refers to the product obtained by refluxing the Na_2MnSiO_4 material (from Figure 2a) with a large excess of LiBr in hexanol for 4 h − 12 h.

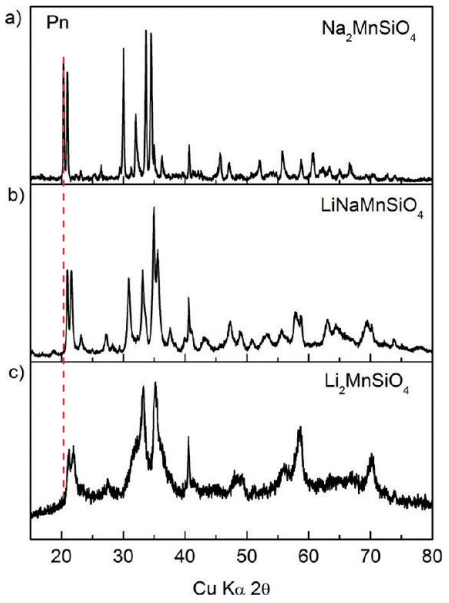

Figure 2. XRD patterns of (a) Na_2MnSiO_4, (b) $LiNaMnSiO_4$, (c) Li_2MnSiO_4.

Figure 2c shows the experimental pattern obtained after heating the $NaMn_2SiO_4$ material at 165 °C for 17 h with an aqueous solution containing a large excess of LiBr in a hydrothermal reactor. Figures. 2a-c clearly show a shift of the main diffraction peaks observed around 20−22 and 29−40° 2θ to higher 2θ values from Figure 2a−c, pointing to a reduction in cell volume as expected from the substitution of Li^+ for Na^+.

3.2.1. Pn-Na_2MnSiO_4. The Rietveld refinement of the Na_2MnSiO_4 product is shown in Figure 3. The main phase contributing to this pattern can be attributed to the *Pn*-Na_2MnSiO_4 structure (JCDPS #55−0638), as expected. In the Rietveld analysis, only lattice parameters were refined for the *Pn*-Na_2MnSiO_4 phase, whereas its atom coordinates were fixed at the optimized ab initio DFT values (Table 1). The final lattice parameters obtained from Rietveld refinement (Figure 3) were a = 7.0395(8) Å, b = 5.5816(6) Å, c = 5.3305(5) Å and β = 89.82(3)°, close to the calculated values obtained by GGA ab initio DFT optimizations that were used as initial cell data for the Rietveld refinement. A minor impurity phase of MnO was detected in this synthesis product, along with a few unidentified weak diffraction peaks at 22.3 and 31.3°2θ. These peaks do not belong to any of the common impurities that could be expected such as Na_2SiO_3, Mn_2SiO_4 or Mn_3O_4.

3.2.2. Pn-$LiNaMnSiO_4$. Different degrees of cationic exchange were obtained depending on the Li/Na ion-exchange method performed on the *Pn*-Na_2MnSiO_4 product. Refluxing the Na_2MnSiO_4 powder in a LiBr solution in hexanol (185 °C, 2−8 h) yielded a product that retained the *Pn* structure of Na_2MnSiO_4 as the main phase (Figure 2b), but had significantly larger lattice parameters than what was calculated by GGA ab initio DFT for Li_2MnSiO_4 (Table 2). Rietveld refinement with TOPAS of the lattice parameters on the experimental powder pattern for the synthesis product shown in Figure 2b yielded refined cell parameters $a \cong 6.888$ Å, $b \cong 5.436$ Å, $c \cong 5.165$ Å, $\beta \cong 89.41°$. The initial cell data were the lattice-parameter values calculated by GGA ab initio DFT, and the atomic coordinates were fixed at the GGA ab initio values for Li_2MnSiO_4. The experimental numbers did not match credibly the GGA-optimized parameters a = 6.2162 Å, b =

dx.doi.org/10.1021/cm202793j | Chem. Mater. 2011, 23, 5446−5456

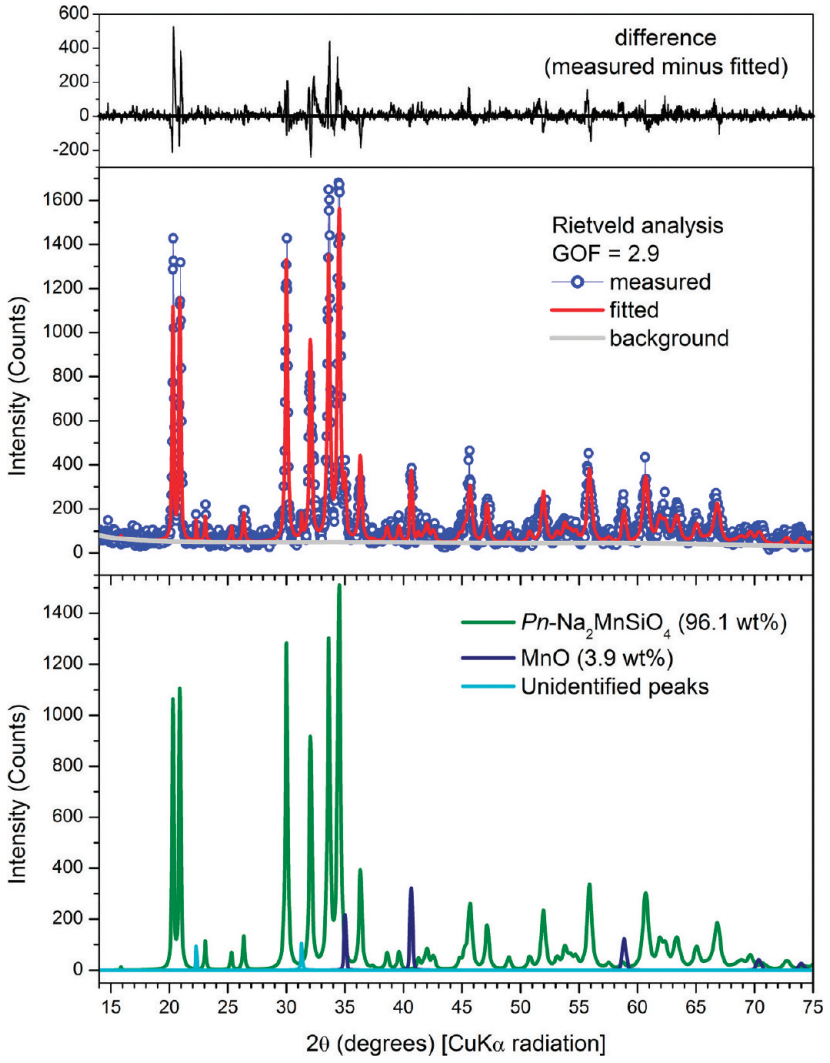

Figure 3. Rietveld refinement of Na_2MnSiO_4.

5.3912 Å, c = 4.9742 Å, β= 89.898° (Table 2). The larger volume of the experimental cell suggested a residual amount of ~50% Na in the synthesized material. In addition, the recalculated and experimental patterns indicated considerable diffraction intensity mismatch around 20−22 and 29−40° 2θ. All this pointed to a possible $LiNaMnSiO_4$ material.

GGA ab initio DFT optimization of the two possible ordered *Pn* crystal structure models for $LiNaMnSiO_4$ showed that one of the two (shown in Table 3) had lower total energy than the other one by 0.2 eV per formula unit. It also matched the experimental pattern quite well (Figure 2b) while the other possible ordered $LiNaMnSiO_4$ structure did not. We therefore suggest that the cell data and fractional coordinates for ordered $LiNaMnSiO_4$ in Table 3 correspond to the synthesized material. The corresponding Rietveld refinement is shown in Figure 4, where only the cell parameters of *Pn*-$LiNaMnSiO_4$ were refined and the atom coordinates were fixed at those calculated by GGA ab initio DFT (Table 3). The refined experimental lattice parameters were a = 6.854(1) Å, b = 5.3932(2) Å, c = 5.1332(7) Å, β= 90.32(3)°, in close agreement with the GGA ab initio DFT values. Compared to Na_2MnSiO_4 (Figure 2a), the peaks shift toward higher angles for $LiNaMnSiO_4$ is clearly visible, except for the peak at 40° corresponding to the MnO impurity phase. Again, this is an indication of the expected decrease in cell volume. There are also in this case some small impurity peaks that could not be identified and that do not match either Mn_3O_4, Mn_2SiO_4, Na_2SiO_3, Li_2SiO_3 or any of the known polymorphs of Li_2MnSiO_4 (*Pmn*2$_1$, *Pmnb*, and *P*2$_1$/*n*).

3.2.3. Pn-Li_2MnSiO_4. Longer refluxing time (up to 12 h) of *Pn*-Na_2MnSiO_4 in a LiBr-hexanol solution did not permit an exchange of the second Na^+ using this ion-exchange technique. Another well-known route to ion exchange is to heat the material in the presence of a lithium salt just above the melting point in Ar. However, attempts to exchange the Na^+ cation for Li^+ cations using several molten salts ($LiNO_3$ at 300 °C, LiI:LiCl; 64:36 at 400 °C) were not successful. A mixture of *Pn* and *Pmn*2$_1$ structures were obtained when using $LiNO_3$ and a full conversion to *Pmn*2$_1$ was obtained when using LiI, demonstrating the limited metastability range of the *Pn* polymorph of Li_2MnSiO_4 upon heating.

Heating the Na_2MnSiO_4 synthesized material (Figure 2a) in an aqueous solution of LiBr under hydrothermal conditions (165 °C, 12 h) successfully converted it to Li_2MnSiO_4. Similar to the Rietveld analysis of *Pn*-Na_2MnSiO_4 (Figure 3) and *Pn*-$LiNaMnSiO_4$ (Figure 4), the Rietveld refinement of *Pn*-Li_2MnSiO_4 shown in Figure 5 assumed atomic positions fixed at GGA *ab initio* DFT values (Table 2), while refining only the

dx.doi.org/10.1021/cm202793j | *Chem. Mater.* 2011, 23, 5446−5456

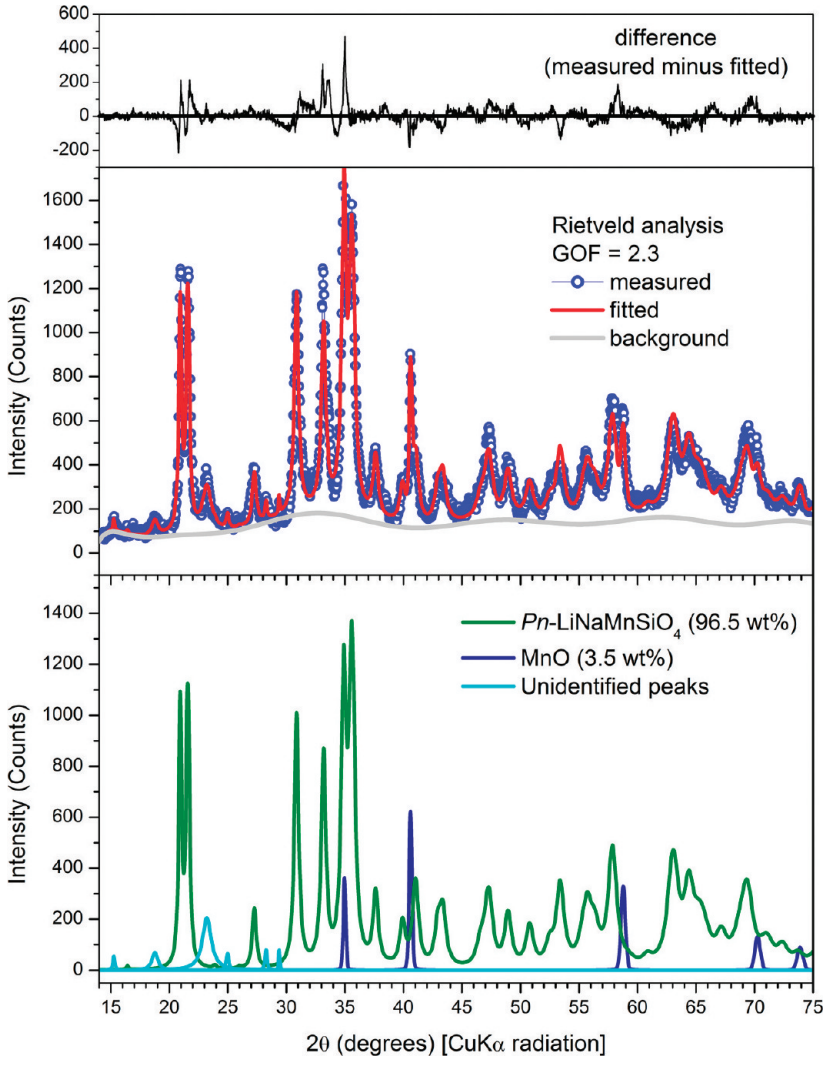

Figure 4. Rietveld refinement of $LiNaMnSiO_4$.

cell parameters. In this case, however, the Rietveld model giving best agreement with the observed XRD pattern required inclusion of a bimodal distribution of crystallite sizes for *Pn*-Li_2MnSiO_4. Both crystallite size ranges were constrained to have the same refined lattice-parameter values using appropriate parameters in the TOPAS software. Additionally, a standard March-Dollase preferred-orientation (PO) correction[25,26] along (010) and (001) directions (as implemented in TOPAS) needed to be applied to the crystallites with larger size. No PO correction was applied to the *Pn* crystallites with small crystallite size producing broader diffraction peaks. This yielded a calculated pattern matching the mix of broad and thin diffraction lines observed for this phase (see Figure 5). This suggests that the *Pn*-Li_2MnSiO_4 synthesis product may indeed have a bimodal distribution in terms of crystallite size, with the larger particles having a nonspherical shape. Final values of experimental lattice parameters refined for the novel *Pn*-Li_2MnSiO_4 polymorph were a = 6.593(5) Å, b = 5.402(1) Å, c = 5.090(2) Å, β= 89. 7(3)°, which corresponds closely to the values obtained by ab initio calculations (Table 2).

3.3. SEM, TEM, EDX, and Bulk Elemental Analysis Results. SEM micrographs of Na_2MnSiO_4 before and after ion-exchange were taken and are shown in Figure 6. The material consists of relatively large (~10 μm) particles mixed with submicrometer crystallites. There is no change in the morphology of the material, except that it seems that the aggregate size is smaller after ion-exchange. The aggregates are probably broken during the hydrothermal ion-exchange treatment resulting in a smaller size.

Figure 7 shows high-resolution TEM micrographs of grains of the *Pn* "Li_2MnSiO_4" material. Figures 7a and b show nanocrystalline blocks with relatively uniform size smaller than 10 nm as well as needles larger than 50 nm. Figure 7c shows a high resolution micrograph single-crystal needles and platelets larger than 50 nm and Figure 7d spherical particles. This set of pictures then supports the bimodal distribution of crystallite sizes that had to be hypothesized in the interpretation of the diffraction pattern in Figure 5.

Figure 8 shows zones 1−4 that were analyzed by EDX during TEM examination. Although Li cannot be analyzed, analyses from zones 1−3 are uniform and consistent with a $Li_{1.9}Na_{0.1}MnSiO_4$ material, based on the Na:Mn:Si ratio. Zone s4 contains no sodium and no silicon, and therefore corresponds to a manganese oxide. This is in line with the ~4 wt % MnO impurity content obtained from the XRD diffraction pattern in Figure 5.

The composition of $Li_{1.9}Na_{0.1}MnSiO_4$ estimated by TEM-EDX is corroborated by bulk elemental analyses performed on

dx.doi.org/10.1021/cm202793j | *Chem. Mater.* 2011, 23, 5446−5456

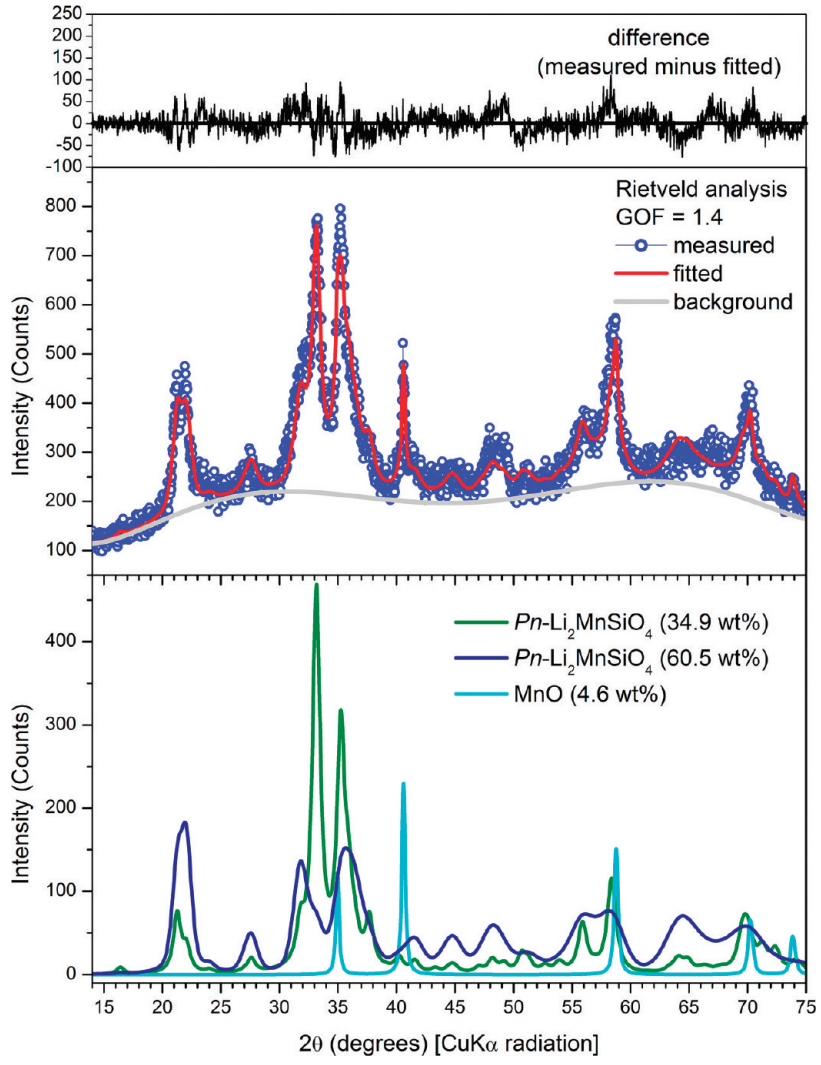

Figure 5. Rietveld refinement of Li_2MnSiO_4 obtained by ion-exchange.

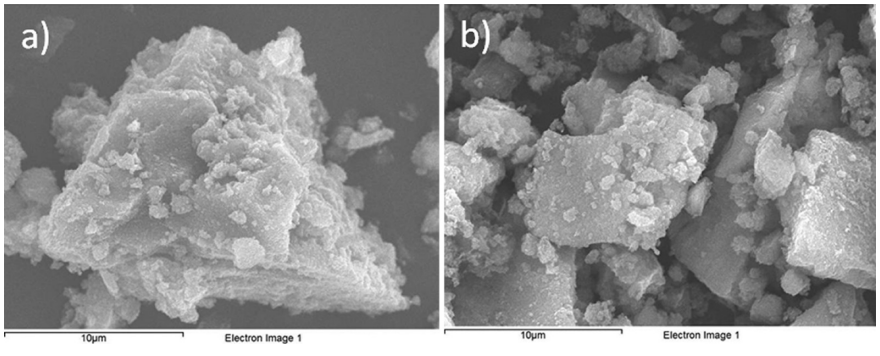

Figure 6. SEM micrographs of (a) Na_2MnSiO_4 and (b) Li_2MnSiO_4 prepared by ion-exchange.

the *Pn*-Li_2MnSiO_4 . An atomic ratio of 1.19(18)for Mn:Si (where the numbers in parentheses are the estimated 2σ standard deviation error) was determined by XRF spectrometry.

3.4. Differential Scanning Calorimetry. The thermal stability of $LiNaMnSiO_4$ and Li_2MnSiO_4 *Pn* polymorphs was investigated by DSC. Upon heating in N_2 at 20 °C/min from 100−500 °C in DSC experiments (Figure 9), no significant variation was observed for $LiNaMnSiO_4$. By contrast, a broad exothermic peak from 150−420 °C, peaking at 275 °C was measured for Li_2MnSiO_4 due to a transformation from *Pn* to $Pmn2_1$. The enthalpy change was estimated at 4.7 ± 0.2 kJ/mol, which agrees reasonably well with total-energy difference of 4.1 kJ/mol obtained from GGA+U calculations (Table 5). As mentioned above, during early attempts to exchange Na^+ for Li^+ by molten salts techniques, it was observed that a mixture of Li_2MnSiO_4 in the *Pn* and $Pmn2_1$ phases were obtained when heating at 300 °C and only $Pmn2_1$ when heating at 400 °C. This is due to the partial or total conversion of the *Pn* phase to the stable $Pmn2_1$ phase. To further confirm this phase transition

dx.doi.org/10.1021/cm202793j | *Chem. Mater.* 2011, 23, 5446−5456

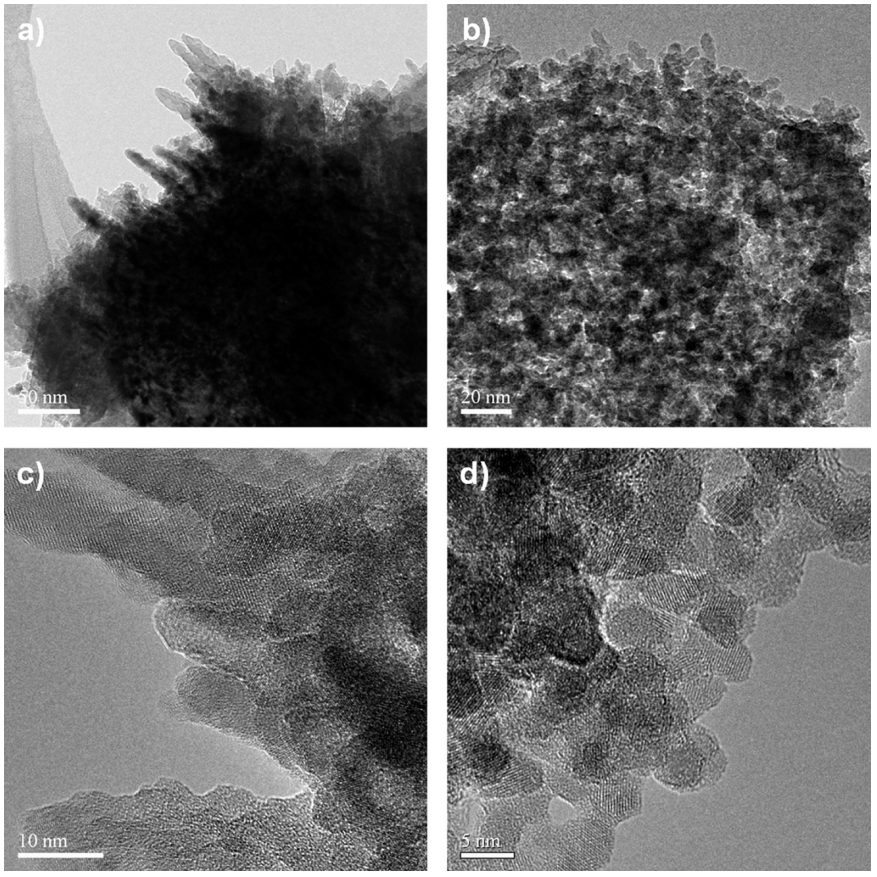

Figure 7. (a) TEM picture of area composed of needle-shaped crystallites; (b) TEM picture of are composed of spherical and some needle-shaped crystallites; (c) HR-TEM showing needle-shaped crystallites; (d) HR-TEM showing crystallites with uniform size smaller than 10 nm.

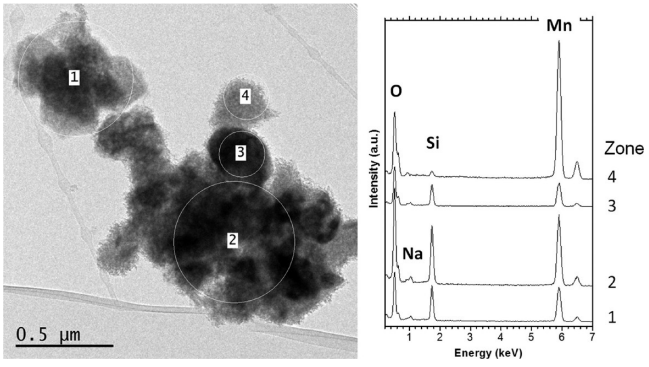

Figure 8. EDX analysis was performed on the four zones 1−4 and corresponding EDX spectra.

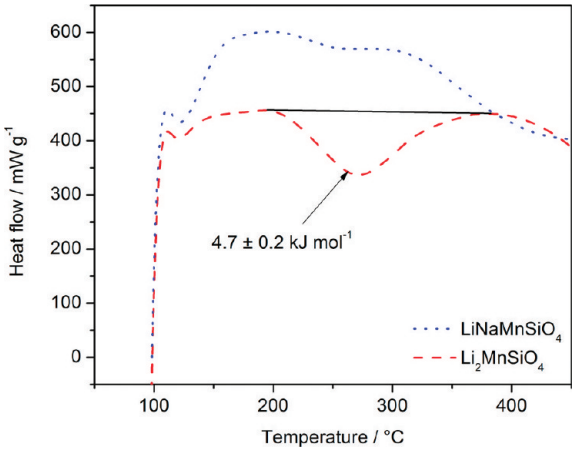

Figure 9. DSC of *Pn* $LiNaMnSiO_4$ (blue dotted line) and Li_2MnSiO_4 (red dashed line).

observed by DSC, the Li_2MnSiO_4 powder in the *Pn* phase obtained by hydrothermal ion-exchange was heated at 400 °C for 4 h in Ar. An XRD pattern was then taken, which also showed that the structure had changed to $Pmn2_1$. This has consequences on the battery assembly, as any carbon coating should be performed before the ion exchange, because a heat treatment of Li_2MnSiO_4 to burn the carbon precursor (typically at 700 °C) would lead to the phase transformation of the *Pn* structure to the more stable $Pmn2_1$ polymorph.

4. ELECTROCHEMICAL CYCLING

4.1. Importance of Carbon Coating. It is well-known that a conductive carbon layer is required in order to study the electrochemical activity of Li_2MnSiO_4, as almost no lithium can be extracted from uncoated Li_2MnSiO_4 due to its low electronic conductivity.[27] A good coating requires heating the carbon precursor under inert atmosphere to at least 650 °C, thus coating cannot be done on *Pn*-Li_2MnSiO_4 as it transforms to the $Pmn2_1$ structure at 300 °C. To avoid this, an in situ carbon coating route was used by adding sucrose during the sol−gel reaction of Na_2MnSiO_4. This resulted in carbon-coated Na_2MnSiO_4 which was exchanged to Li_2MnSiO_4 and used for the electrochemical measurements. In situ carbon-coated $Pmn2_1$-Li_2MnSiO_4 was prepared in the same manner to serve as a comparison.

dx.doi.org/10.1021/cm202793j | *Chem. Mater.* 2011, 23, 5446−5456

4.2. GGA+U versus Experimental Evaluation of Equilibrium Voltages. As pointed out above in §3.1 (Table 4), for the extraction of a first lithium atom accompanied by oxidation of Mn^{2+} to Mn^{3+} in the $Pmn2_1$ phase, we obtained a calculated voltage of 4.23 V compared to a value of 4.12 V from Figure 2 in Arroyo et al.[2] It therefore appears that calculated voltages can be reproduced to within ±0.1 V using GGA+U ab initio calculations with VASP.[19,20] Arroyo et al.[2] measured a voltage of 4.2 V for the first Li extracted in the $Pmn2_1$ phase, which agrees well with our measurements, as shown in Figure 10. Both Li_2MnSiO_4

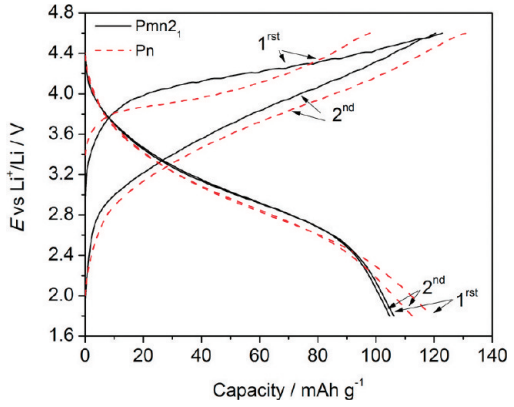

Figure 10. Charge−discharge profile of $Pmn2_1$ (black line) and *Pn* (red dashed line) Li_2MnSiO_4.

polymorphs were cycled galvanostatically between 1.8 and 4.6 V. The 4.6 V limit was chosen as it was found in preliminary experiments that a higher voltage limit leads to rapid deterioration of the electrolyte. The charge plateau for the first cycle of the $Pmn2_1$ polymorph is around 4.2 V while it is lower, ca. 3.9 − 4 V for the *Pn* polymorph. The 4.2 V observed for the $Pmn2_1$ polymorph seems to be in agreement with the experimental value reported by Muraliganth et al.[28] as well as the measured and DFT-calculated voltages reported by Arroyo et al.[2] mentioned above. In the case of the *Pn* polymorph, Figure 10 suggests that lithium extraction from Li_2MnSiO_4 occurs first at a slightly lower potential in the *Pn* structure than in the $Pmn2_1$ structure, in spite of calculations that predicted a similar lithium extraction potential for both polymorphs (Table 4). This could be due to the presence of residual Na^+ in the structure which was suggested by EDX measurements. As shown in Table 4, there is an expected decrease in the voltage associated with the replacement of Li by Na, i.e., $LiNaMnSiO_4$ extraction voltage is predicted to be 4.02 V vs 4.2 V for Li_2MnSiO_4. The discharge profiles and charge profiles after the first cycle are however similar for both polymorphs and do not change during the subsequent cycles. The fact that the charge curves for the two polymorphs differ only during the first cycle, while the discharge curves are similar, suggests that the *Pn* structure undergoes a change during the first extraction of lithium. This is likely due to some degree of amorphization, similar to what was suggested in the case of the $Pmn2_1$ material.[29] The discharge capacity for the *Pn* polymorph is slightly higher than its corresponding charge, which could be explained by a partial oxidation of Mn^{2+} to Mn^{3+} during the hydrothermal ion-exchange.

4.3. Assessment of Capacity Fades. Discharge capacities obtained by galvanostatic cycling are shown in Figure 11 . The

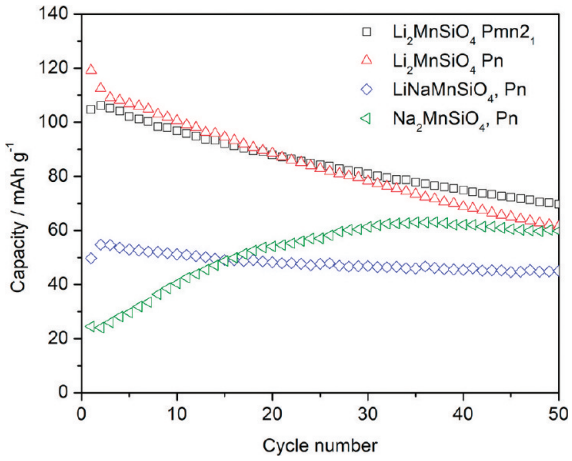

Figure 11. Comparison of the discharge capacity of Li_2MnSiO_4 in the $Pmn2_1$ structure (black squares) and Pn structure (red triangles), $LiNaMnSiO_4$ (blue diamonds) and Na_2MnSiO_4 (green triangles).

discharge capacities observed for the two Li_2MnSiO_4 polymorphs are quite similar, as are the capacity fades. There is a slight advantage for the *Pn* structure in the first cycles (120 mA h g^{-1} vs 100 mA h g^{-1}). Those values are comparable to the capacities obtained in the literature[12] with comparable cycling conditions, and in both cases only the first lithium is extracted, i.e., only the $Mn^{2+} \rightarrow Mn^{3+}$ oxidation is observed. Higher capacities have been reported, for example 200 mA h g^{-1} by Muraliganth et al.,[28] but in their case the cycling limit was higher (4.7 V) while the active material content was lower (75%) and the carbon content higher (20%) than in our case, which could improve the capacity. An improvement in the carbon coating of our material might increase the capacity. After 20 cycles, as shown in Figure 11, the capacities are similar (90 mA h g^{-1} for both polymorphs) and the *Pn* structure yields 62 mA h g^{-1} after 50 cycles compared to 70 mA h g^{-1} for the $Pmn2_1$ structure. Although the framework vs. layered structure of the *Pn* vs. $Pmn2_1$ delithiated materials was anticipated to lead to better stability for the delithiated silicate, this was not observed under our experimental conditions. Rather, it seems that both polymorphs undergo gradual structural changes, possibly amorphization,[29] limiting the reinsertion of lithium. The half exchanged $LiNaMnSiO_4$ exhibits a much lower capacity, at 49 mA h g^{-1}, but is remarkably stable: a capacity of 45 mA h g^{-1} is still measured after 50 cycles. It is not clear if this superior stability is due to the remaining Na^+ in the structure or the fact that less Li^+ is extracted from the structure during cycling. Further studies will be conducted to improve the lithium extraction and investigate why the half-lithiated material is more stable than the fully lithiated one. Work on Na_2FePO_4F has shown that Na^+ can be exchanged electrochemically by cycling in a lithium cell configuration with a Li foil as counter electrode and $LiPF_6$ salt.[30] The capacity reached in that case was almost theoretical and one Na^+ ion was immediately replaced by one Li^+ after the first cycle. In the case of our Na_2MnSiO_4 cycled directly in a lithium battery (see Figure 11), the initial capacity is much lower, 23 mA h g^{-1} for the first cycle, increasing to 60 mA h g^{-1} after 50 cycles. It is likely that there is a gradual exchange of Na^+ ion for Li^+ in the structure given the relative excess of Li^+ to Na^+ in the electrolyte.

Cyclic voltammetry experiments were carried out on the two Li_2MnSiO_4 polymorphs and $LiNaMnSiO_4$ in order to better

dx.doi.org/10.1021/cm202793j | *Chem. Mater.* 2011, 23, 5446–5456

visualize the oxidation and reduction processes (Figure 12). As was observed in the case of the galvanostatic cycling (Figure 11), the lithium extraction potential during the first cycle is lower for the *Pn* polymorph than the *Pmn*2$_1$ polymorph. In both polymorphs, the integration of the oxidation peaks yields a capacity of ca. 85 mA h g^{-1}, indicating that less than one lithium can be removed in these conditions, and less than what is observed in galvanostatic cycling. It is not surprising, however, as 0.1 mV s^{-1} is a relatively fast charging rate, equivalent to *C*/8. On the other hand, the lithium insertion is not significantly different in the *Pn* structure compared to the *Pmn*2$_1$ one, at 2.8 V. During the second cycle, the oxidation peaks are shifted toward lower potentials for both polymorphs and the difference between the oxidation potential of the two polymorphs is reduced significantly. In the case of $LiNaMnSiO_4$, a small peak is visible at 4.2 V, intermediate between the position of the peak of *Pn* and *Pmn*2$_1$ Li_2MnSiO_4, whereas a second peak at 4.8 V is also visible during the first charge. Both Li^+ and Na^+ can be extracted, and it is not clear if both atoms are mobile. However, only a small peak is observed around 3.5 V on discharge, indicating that the amount of Li^+ that can be reinserted in the structure is limited.

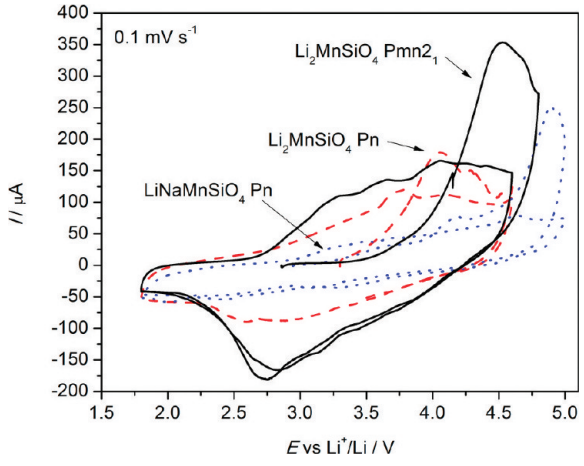

Figure 12. Comparison of cyclic voltammograms of Li_2MnSiO_4 in the Pn structure (dashed red) and Pmn2$_1$ structure (solid black) and $LiNaMnSiO_4$ in the Pn structure (dotted blue).

5. CONCLUSION

We report the synthesis of a new *Pn* polymorph of Li_2MnSiO_4 prepared by ion exchange from Na_2MnSiO_4 and a mixed silicate, $LiNaMnSiO_4$, prepared by partial exchange from Na_2MnSiO_4. The structures were assigned to the *Pn* space group, similar to Na_2MnSiO_4. The new materials $LiNaMnSiO_4$ and Li_2MnSiO_4 as well as Na_2MnSiO_4 were characterized by comparison of X-ray diffraction patterns with patterns generated from DFT calculations for such materials. DSC experiments revealed that the *Pn*-Li_2MnSiO_4 prepared by ion-exchange was stable up to 370 °C. A carbon-coating was added in situ during the synthesis to improve the electrochemical performance. Lithium extraction occurs first at 3.8 V with this polymorph compared to 4.2 V with the *Pmn*2$_1$ polymorph of Li_2MnSiO_4. The discharge capacity is however similar with both polymorphs and although the delithiated structure was anticipated to be more stable than the *Pmn*2$_1$ polymorph because of the framework structure of the *Pn* polymorph vs. the layered structure of the *Pmn*2$_1$ polymorph, the *Pn* Li_2MnSiO_4 suffers from similar capacity loss upon cycling. A limited but stable capacity is obtained by cycling $LiNaMnSiO_4$ (i.e., half-exchanged Na_2MnSiO_4). Partial Li^+ exchange can be performed electrochemically by cycling Na_2MnSiO_4 in a lithium cell, and a capacity of 60 mA h g^{-1} after 50 cycles was obtained in this way.

AUTHOR INFORMATION

Corresponding Author

*E-mail: yaser.abu-lebdeh@nrc-cnrc.gc.ca.

ACKNOWLEDGMENTS

This work was partially supported by Natural Resources Canada's Program of Energy Research and Development under the Electric Mobility Program. The authors thank Bussaraporn Patarachao for XRF measurements and Dave Kingston for SEM.

REFERENCES

(1) Nytén, A.; Abouimrane, A.; Armand, M.; Gustafsson, T.; Thomas, J. O. *Electrochem. Commun.* **2005**, *7*, 156−160.
(2) Arroyo-de Dompablo, M. E.; Armand, M.; Tarascon, J. M.; Amador, U. *Electrochem. Commun.* **2006**, *8*, 1292−1298.
(3) Nishimura, S.-i.; Hayase, S.; Kanno, R.; Yashima, M.; Nakayama, N.; Yamada, A. *J. Am. Chem. Soc.* **2008**, *130*, 13212−13213.
(4) Dominko, R.; Bele, M.; Gaberscek, M.; Meden, A.; Remskar, M.; Jamnik, J. *Electrochem. Commun.* **2006**, *8*, 217−222.
(5) Sirisopanaporn, C.; Boulineau, A.; Hanzel, D.; Dominko, R.; Budic, B.; Armstrong, A. R.; Bruce, P. G.; Masquelier, C. *Inorg. Chem.* **2010**, *49*, 7446−7451.
(6) Armstrong, A. R.; Lyness, C.; Ménétrier, M.; Bruce, P. G. *Chem. Mater.* **2010**, *22*, 1892−1900.
(7) Mali, G.; Meden, A.; Dominko, R. *Chem. Commun.* **2010**, *46*, 3306−3308.
(8) Politaev, V. V.; Petrenko, A. A.; Nalbandyan, V. B.; Medvedev, B. S.; Shvetsova, E. S. *J. Solid State Chem.* **2007**, *180*, 1045−1050.
(9) Arroyo-de Dompablo, M. E.; Dominko, R.; Gallardo-Amores, J. M.; Dupont, L.; Mali, G.; Ehrenberg, H.; Jamnik, J.; Morán, E. *Chem. Mater.* **2008**, *20*, 5574−5584.
(10) Sirisopanaporn, C.; Masquelier, C.; Bruce, P. G.; Armstrong, A. R.; Dominko, R. *J. Am. Chem. Soc.* **2011**, *135*, 1263−1265.
(11) Lyness, C.; Delobel, B.; Armstrong, A. R.; Bruce, P. G. *Chem. Commun.* **2007**, 4890−4892.
(12) Dominko, R.; Bele, M.; Kokalj, A.; Gaberscek, M.; Jamnik, J. *J. Power Sources* **2007**, *174*, 457−461.
(13) Bruce, P.; Robert Armstrong, A.; L. Gitzendanner, R. *J. Mater. Chem.* **1999**, *9*, 193−198.
(14) Fuchs, B.; Kemmler-Sack, S. *Solid State Ionics* **1994**, *68*, 279−285.
(15) Meng, Y. S.; Arroyo-de Dompablo, M. E. *Energy Environ. Sci.* **2009**, *2*, 589−609.
(16) Rietveld, H. *Acta Crystallogr.* **1967**, *22*, 151−152.
(17) *TOPAS Version 4.2*; Bruker AXS: Madison, WI.
(18) Vaivars, G.; Grins, J.; Hörlin, T. *Solid State Ionics* **1995**, *78*, 259−267.
(19) Kress, G. Ph. D. thesis, Technische Universität Wien, Wien, Germany, 1993.
(20) Kresse, G.; Hafner, J. *Phys. Rev. B* **1993**, *48*, 13115.
(21) Vosko, S. H.; Wilk, L.; Nusair, M. *Can. J. Phys.* **1980**, *58*, 1200−1211.
(22) Mercier, P. H. J.; Le Page, Y. *Acta Crystallogr., Sect. B* **2008**, *64*, 131−143.
(23) Le Page, Y.; Rodgers, J. R. *J. Appl. Crystallogr.* **2005**, *38*, 697−705.
(24) Zhou, F.; Cococcioni, M.; Kang, K.; Ceder, G. *Electrochem. Commun.* **2004**, *6*, 1144−1148.
(25) March, A. *Z. Kristallogr.* **1932**, *81*, 285−297.

(26) Dollase, W. *J. Appl. Crystallogr.* **1986**, *19*, 267−272.
(27) Belharouak, I.; Abouimrane, A.; Amine, K. *J. Phys. Chem. C* **2009**, *113*, 20733−20737.
(28) Muraliganth, T.; Stroukoff, K. R.; Manthiram, A. *Chem. Mater.* **2010**, *22*, 5754−5761.
(29) Kokalj, A.; Dominko, R.; Mali, G.; Meden, A.; Gaberscek, M.; Jamnik, J. *Chem. Mater.* **2007**, *19*, 3633−3640.
(30) Ellis, B. L.; Makahnouk, W. R. M.; Makimura, Y.; Toghill, K.; Nazar, L. F. *Nat. Mater.* **2007**, *6*, 749−753.